Numerical study of the combined stroke swimmer in an incompressible fluid

Kumar, Aditya; Pourquie, Mathieu; Tam, Daniel See Wai; Ooms, Gijsbert

DOI
10.1088/1873-7005/ab793b

Publication date
2020

Document Version
Final published version

Published in
Fluid Dynamics Research

Fluid Dynamics Research

The Japan Society of Fluid Mechanics

PAPER

Numerical study of the combined stroke swimmer in an incompressible fluid

IOP Publishing | The Japan Society of Fluid Mechanics Fluid *Dynamics* Research

Fluid Dyn. Res. **52** (2020) 025505 (19pp) https://doi.org/10.1088/1873-7005/ab793b

Numerical study of the combined stroke swimmer in an incompressible fluid

Aditya Kumar, Mathieu Pourquie, Daniel See-Wai Tam and Gijsbert Ooms[1]

JM Burgerscentrum, Delft University of Technology, Faculty of Mechanical Engineering, Laboratory for Aero- & Hydrodynamics, Mekelweg 2, 2628 CD Delft, The Netherlands

E-mail: g.ooms@tudelft.nl

Received 27 September 2019, revised 14 February 2020
Accepted for publication 24 February 2020
Published 17 March 2020

Abstract

A numerical simulation has been made of the combined stroke swimmer (a deformable sphere) and compared with the results of the second-order perturbation theory of Felderhof and Jones (2017). At a small ratio of the amplitude of the deformation of the sphere and the radius of the sphere the numerical and theoretical results agree well. However for a larger value of this ratio the results deviate due to inertia. The streamlines, as calculated numerically, change significantly with increasing inertia.

Keywords: micro-swimmer, numerical simulation, inertial locomotion

1. Introduction

Significant attention has already been paid to the influence of inertia on a micro-swimmer. Fluid inertia is of importance to the locomotion of organisms with sizes O (1 mm–20 mm). Several papers are devoted to this problem. A brief review of some of them is given below.

For instance Wang and Ardekani (2012) investigated theoretically the convective inertial force on the squirmer: a model swimming organism that achieves locomotion via tangential movement of its surface, neglecting radial displacement. There are two kinds of squirmer swimmers: a puller for which the thrust is generated in front of the swimmer and a pusher for which the thrust is behind the swimmer. Wang and Ardekani (2012) found that the swimming speed of a pusher swimmer increases due to the effect of inertia, whereas the puller is hindered by inertia. For both kinds of swimmers the swimming speed is calculated as a

[1] Author to whom any correspondence should be addressed.

function the Reynolds number ($Re = LU/\nu$: L the characteristic length of the swimmer, U its velocity and ν the kinematic velocity of the fluid).

Ishimoto (2013) discussed four dimensionless parameters which influence the swimmer: the Reynolds number ($Re = LU/\nu$), the oscillatory Reynolds number ($R_\omega = L^2/\nu T$) in which T is the characteristic time scale of the swimmer, the Stokes number $R_S = (\rho_p/\rho_f)R_\omega$ in which ρ_p and ρ_f are the densities of the swimmer and the fluid respectively and finally $R_g = (R_S - R_\omega)gT/U$ in which g is the gravity acceleration. In the paper a literature review for different values of the four parameters is given. Ishimoto (2013) also made a theoretical study of unsteady inertial effects on the motion of a spherical micro-swimmer with small deformation of the surface. To that purpose he applied a squirmer in unsteady Stokes flow. The inertial effects on the swimming velocity are significant for a flapping swimmer, whereas there is a slight influence for a swimmer with a wave pattern.

Khair and Chisholm (2014) used matched asymptotic expansions at small Reynolds numbers to calculate the swimming velocity of the spherical squirmer through second-order expansion of the Reynolds number. An expression is derived for the speed of propulsion of the swimmer as a function of the Reynolds number. They also calculated the velocity and vorticity fields around the squirmer.

Li and Ardekani (2014) studied numerically the dynamics of a single squirmer near a no-slip wall at low Reynolds numbers. Different modes are found for a single squirmer and the inertial effects are important. The squirmer can escape from the wall, it can flow along the wall with constant distance and it can have a periodic trajectory. The behaviour of multiple squirmers between two walls is very different from the behaviour of a single one. Near the wall at a relatively small concentration a collection of squirmers tend to cluster. At high concentration a part of the squirmers is located close to the wall and the remaining part in the bulk region. Close to the wall the squimers tend to orient in the direction normal to the wall, whereas in the bulk they are in the direction parallel to the wall.

Chisholm *et al* (2016) investigated numerically the 2D and 3D flow around a squirmer for Reynolds numbers between 0.01 and 1000, where the influence of inertia is important. There are profound differences in the locomotion of a pusher and puller. The swimming speed of a pusher increases monotonically with Re. Convection of vorticity past the pusher's surface causes a steady axisymmetric flow that remains stable up to at least $Re = 1000$. In contrast, the swimming speed of a puller is non-monotonic with Re. A puller traps vorticity within its wake, which leads to flow instabilities that cause a decrease in the time-averaged swimming speed at large Re. The unsteady 3D flow simulations show the transition of the flow around the squirmer from steady and axisymmetric to unsteady and 3D.

Dombrowski *et al* (2019) made a numerical study of the spherobot: two unequal size spheres that oscillate in anti-phase generating nonlinear steady streaming flows. These flows enable the swimmer to propel itself, and also switch direction as the Reynolds number increases. Analyzing the flow fields, Dombrowski *et al* (2019) showed that the transition in swimming direction corresponds to the reversal of the streaming flows around the spherobot that occurs as the Reynolds number increases.

Felderhof and Jones studied theoretically in a number of publications (see for instance Felderhof and Jones 2017) the swimming of a sphere immersed in a viscous incompressible fluid with inertia for periodic surface modulations on the basis of the Navier–Stokes equations. As an example their combined stroke swimmer in an axisymmetric geometry (see Felderhof 2015) is shown in figure 1 for the dimensionless time (time:t; time period of the surface modulation: T_c), as a function of the dimensionless coordinates (axial coordinate z, radial coordinate r) and radius of the swimmer a. From (a) to (d) (see figure 1) the swimmer develops as a function of time from a deformed sphere extended in horizontal direction into a

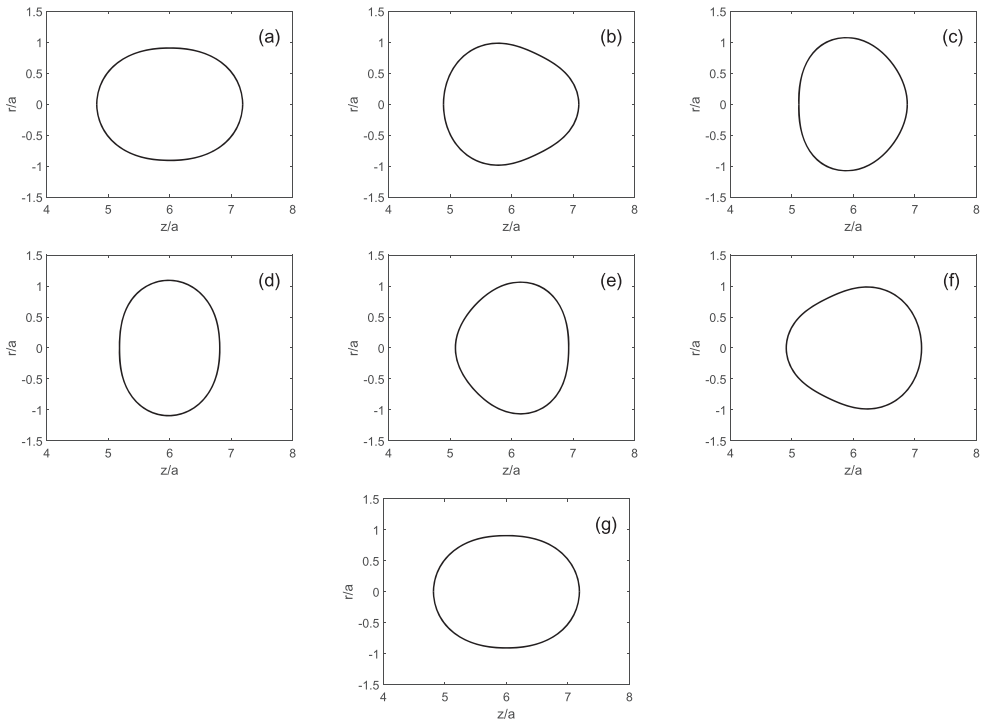

Figure 1. Combined stroke swimmer as a function of time for (*a*): $t/T_c = 0$, (*b*): $t/T_c = 1/6$, (*c*): $t/T_c = 2/6$, (*d*): $t/T_c = 3/6$, (*e*): $t/T_c = 4/6$, (*f*): $t/T_c = 5/6$, (*g*): $t/T_c = 1$.

deformed sphere extended in vertical direction. From (*d*) to (*g*) the swimmer returns again to the deformed sphere extended in horizontal direction. The volume of the swimmer remains the same all the time. When starting from $t = 0$ the velocity of the swimmer during the period from (*a*) to (*d*) is in the left direction, the velocity increases from 0 to a maximum (negative) value and then returns to a small value. During the period from (*d*) to (*g*) the velocity is the right direction, it increases to a maximum (positive) value and then returns again to a small value. The positive velocity amplitude during the period (*d*)–(*g*) is larger than the negative velocity amplitude during the period (*a*)–(*d*). So the mean value of the velocity of the swimmer is in the (positive) right direction. The details will be given during the discussion about the results. Felderhof and Jones (2017) calculate the mean swimming velocity and other properties in terms of the surface modulation and the fluid viscosity. They find that the optimal swimming efficiency depends on a dimensionless scaling number involving the radius of the sphere, the time period of the swimmer and the kinematic viscosity of the fluid ν. This scaling number (which is similar to the oscillatory Reynolds number $R_\omega = L^2/\nu T$ discussed by Ishimoto (2013)) is a measure of the inertia. It has a strong influence on the velocity of the swimmer.

One of the aims of this paper is to compare numerical results with the results of the analytical calculation for the combined stroke swimmer of Felderhof and Jones (2017) as a function of the amplitude of the surface modulation. The expectation is that for small amplitudes the results of the numerical simulation and theory agree well, but that for larger values of the surface modulation the results will deviate as the theory of Felderhof and Jones

(2017) is based on a (second-order) perturbation calculation. The advantage of the numerical simulation is that the influence of larger amplitudes can be studied. We will calculate for the combined stroke swimmer (in an axisymmetric geometry) the mean swimming velocity and the velocity oscillations due to the time-dependent movement of the swimmer and compare these with the analytical results of Felderhof and Jones (2017) for two values of the dimensionless amplitude ($\delta/a = 0.025$ and $\delta/a = 0.050$: δ is the modulation amplitude and a the swimmer radius) of the surface modulation.

Special attention will be paid to the influence of inertia. By decreasing the viscosity of the fluid (keeping all other parameters the same) the influence of the velocity on the swimmer, of the inertia and of the Reynolds number will be calculated.

2. Numerical method

The code uses the immersed boundary method (IBM). A staggered grid is applied and the code uses the finite volume scheme. The Navier–Stokes equation is solved numerically for the axisymmetric combined stroke swimmer in a reference system which is co-moving with the swimmer. (At every time step the force on the swimmer is calculated. This force could lead to an acceleration of the swimmer. However this acceleration is incorporated with a negative sign in the Navier–Stokes equation, which keeps the swimmer at the same position and causes a velocity field far from the swimmer.)

$$\frac{\partial \mathbf{u}}{\partial t} + \mathbf{u} \cdot \nabla \mathbf{u} = -\frac{1}{\rho}\nabla p + \nu(\nabla^2 \mathbf{u}) + \mathbf{f}_i + \mathbf{f}, \tag{1}$$

where ρ is the fluid density, $\mathbf{u}$ the fluid velocity, t the time, p the pressure, ν the kinematic viscosity of the fluid, $\mathbf{f}_i$ the inertial force due to the co-moving reference system and $\mathbf{f}$ the forcing term due to the interaction of the swimmer with the fluid. Using Gauss divergence theorem, the integrals for momentum, and diffusion are converted to surface integrals. They are then evaluated over the surface of a grid cell as shown in equation (2)

$$\int_V \frac{\partial \mathbf{u}}{\partial t} \mathrm{d}V + \int_V \nabla \cdot (\mathbf{u}\mathbf{u}) \mathrm{d}V = -\int_V \frac{1}{\rho}\nabla p \mathrm{d}V + \int_V \nu(\nabla^2 \mathbf{u}) \mathrm{d}V + \int_V \mathbf{f}_i \mathrm{d}V + \int_V \mathbf{f} \mathrm{d}V, \tag{2}$$

Integration of equation (2) in time is done in parts. In the first part an intermediate velocity $\mathbf{u}^*$ is obtained from a guessed value of the pressure field $p^{n-1/2}$ as used in equation (3). The symbols $\mathbf{A}^n$ and $\mathbf{D}^n$ denote the advection and diffusion terms at the old time levels respectively, $\mathbf{F}_i^n$ is the inertial force due to the co-moving reference system, Δt indicates the time step and ν indicates the kinematic viscosity of the fluid. ($\mathbf{A}^n$, $\mathbf{D}^n$ and $\mathbf{F}_i^n$ are surface integrals over a grid cell. n reperesents the time level.) This intermediate velocity $\mathbf{u}^*$ is not divergence free. In order to correct this, a pressure that corresponds to an intermediate divergence free velocity field is obtained (equation (4)) and the intermediate velocities are corrected to obtain the velocities at the next time step (equation (5)). The guessed value of the pressure field $p^{n-1/2}$ is also corrected to obtain the pressure at the new time level (equation (6))

$$\frac{\mathbf{u}^* - \mathbf{u}^n}{\Delta t} = -\left(\frac{1}{\rho}\nabla p^{n-1/2} - \mathbf{A}^n + \nu \mathbf{D}^n + \mathbf{F}_i^n\right), \tag{3}$$

$$\frac{1}{\rho}\nabla^2\tilde{p} - \frac{1}{\Delta t}\nabla\cdot\mathbf{u}^* = 0, \tag{4}$$

$$\mathbf{u}^{n+1} = \mathbf{u}^* - \Delta t\frac{1}{\rho}\nabla\tilde{p}, \tag{5}$$

$$p^{n+1/2} = p^{n-1/2} + \tilde{p}. \tag{6}$$

In the immersed boundary method the above equations are modified to account for the presence of an obstacle (the swimmer) in the calculation domain. The intermediate velocity computed from equations (3)–(6) is modified by a forcing term $\mathbf{f}^{n+1/2}$ into a second intermediate velocity $\mathbf{u}^{**}$ at the location of the obstacle (equation (8)). The velocities at the new time level are obtained from the pressure (equation (10)). The scheme is given by equations (7)–(11). This is known as a fully explicit scheme

$$\frac{\mathbf{u}^* - \mathbf{u}^n}{\Delta t} = -\left(\frac{1}{\rho}\nabla p^{n-1/2} - \mathbf{A}^n + \nu\mathbf{D}^n + \mathbf{F}_i^n\right), \tag{7}$$

$$\mathbf{u}^{**} = \mathbf{u}^* + \Delta t\,\mathbf{f}^{n+1/2}, \tag{8}$$

$$\frac{1}{\rho}\nabla^2\tilde{p} - \frac{1}{\Delta t}\nabla\cdot\mathbf{u}^{**} = 0, \tag{9}$$

$$\mathbf{u}^{n+1} = \mathbf{u}^{**} - \Delta t\frac{1}{\rho}\nabla\tilde{p}, \tag{10}$$

$$p^{n+1/2} = p^{n-1/2} + \tilde{p}. \tag{11}$$

A fully explicit scheme given by equations (7)–(11) has one major disadvantage. It does not allow for large time steps. The diffusion and the Courant criteria for restrictions on the time steps for the fully explicit scheme are given by equations (12) and (13) respectively. The diffusion criterion is more restrictive as compared to the Courant criterion. The time-step Δt for the diffusion criterion (equation (12)) is proportional to the square of the grid spacing (Δx, Δy), while the Courant criterion (equation (13)) is less restrictive with Δt varying linearly as the grid spacing. Hence, extremely small time steps are required to solve the equations (7)–(11). This restriction on the time-step can be overcome by using an implicit scheme for the diffusion term. Hence, for regimes which are highly viscous an implicit treatment of the diffusion term is preferred

$$\frac{\nu\Delta t}{\mathrm{d}x^2} + \frac{\nu\Delta t}{\mathrm{d}y^2} \leqslant 0.5 \tag{12}$$

and

$$\frac{U\Delta t}{\mathrm{d}x} + \frac{V\Delta t}{\mathrm{d}y} \leqslant C_{\max}. \tag{13}$$

So in order to overcome the restrictions posed by a fully explicit scheme an implicit integration for the diffusion terms is used. This scheme is given by equations (14)–(18). A Crank–Nicholson scheme is used for the implicit integration of the diffusion terms, while the advection terms are integrated through a second-order Adams–Bashforth scheme, which consists of using the advection terms from the current and the old time level respectively ($\mathbf{A}^n$, $\mathbf{A}^{n-1}$). In addition to this, extra terms to the pressure correction equation (18) are added due to

the diffusion terms being implicitly solved

$$\frac{\mathbf{u}^* - \mathbf{u}^n}{\Delta t} = \frac{\nu}{2}\nabla^2(\mathbf{u}^n + \mathbf{u}^*) - \frac{1}{\rho}\nabla p^{n-1/2} - \left(\frac{3}{2}\mathbf{A}^n - \frac{1}{2}\mathbf{A}^{n-1}\right), \tag{14}$$

$$\mathbf{u}^{**} = \mathbf{u}^* + \Delta t \mathbf{f}^{n+1/2}, \tag{15}$$

$$\frac{1}{\rho}\nabla^2\tilde{p} - \frac{1}{\Delta t}\nabla \cdot \mathbf{u}^{**} = 0, \tag{16}$$

$$\mathbf{u}^{n+1} = \mathbf{u}^{**} - \Delta t\frac{1}{\rho}\nabla\tilde{p}, \tag{17}$$

$$p^{n+1/2} = p^{n-1/2} + \tilde{p} - \frac{\nu}{2}\Delta t\nabla^2\tilde{p}. \tag{18}$$

The volume penalization IBM of Kajishima *et al* (2001) has been implemented.The forcing term $\mathbf{f}$ in this IBM is computed from the mass fraction (α) occupied by the (partially) immersed object in a cell where n denotes the time level (see equation (19)). $\mathbf{U}_{\text{solid}}^{n+1}$ and $\mathbf{u}^*$ are the velocities of the swimmer at the fluid-solid interface and the fluid in the cell volume respectively

$$\mathbf{f}^{n+1/2} = \alpha^{n+1}\left(\frac{\mathbf{U}_{\text{solid}}^{n+1} - \mathbf{u}^*}{\Delta t}\right). \tag{19}$$

A rectangular domain is chosen as: ($z/a = -6$ to $z/a = 6$; $r/a = 0$ to $r/a = 6$) (z is the axial coordinate, r the radial coordinate and a is the radius of the swimmer). The swimmer is located at ($z/a = 0$; $r/a = 0$). The reference frame used is that of the swimmer. As explained at every time step the force on the swimmer is calculated. This force could lead to an acceleration of the swimmer. However this acceleration is incorporated with a negative sign in the Navier–Stokes equation, which keeps the swimmer at the same position and causes a velocity field far from the swimmer. Far from the swimmer the velocity is independent of position; it depends of course on time. In the axial direction there are 1200 grid points and in the radial direction 600.

3. Combined stroke swimmer

As mentioned we study one of the micro-swimmers of Felderhof and Jones (2017): the combined stroke swimmer. In Felderhof (2015) the details of this swimmer are given. For the sake of the readability of our paper we give a brief summary of section II of Felderhof's paper (2015).

In spherical coordinates $\mathbf{r}(\mathrm{r}, \theta, \phi)$ the flow velocity $\mathbf{v}(\mathbf{r}, t)$ can be expanded in terms of a set of fundamental solutions $\mathbf{u}_l(\mathrm{r}, \theta)$ and $\mathbf{v}_l(\mathrm{r}, \theta)$ of the Stokes equations

$$\mathbf{v}(\mathbf{r}, t) = -\mathbf{U}(t)\mathbf{e}_z + \sum_{l=1}^{\infty} m_l(t)\mathbf{u}_l(r, \theta) + \sum_{l=2}^{\infty} k_l(t)\mathbf{v}_l(r, \theta)], \tag{20}$$

with

$$\mathbf{u}_l(r, \theta) = \left(\frac{a}{r}\right)^{l+2}[(l+1)P_l(\cos\theta)\mathbf{e}_r + P_l^1(\cos\theta)\mathbf{e}_\theta], \tag{21}$$

$$\mathbf{v}_l(r,\,\theta) = \left(\frac{a}{r}\right)^l \left[(l+1)P_l(\cos\theta)\mathbf{e}_r + \frac{l-2}{l}P_l^1(\cos\theta)\mathbf{e}_\theta\right], \tag{22}$$

a is the radius of the swimmer, $m_l(t)$ and $k_l(t)$ represent the periodic time dependence of the swimmer, $\mathbf{e}_r$ and $\mathbf{e}_\theta$ are the unit vectors in radial and tangential direction respectively. $P_l(\cos\theta)$ are Legendre polynomials and $P_l^1(\cos\theta)$ associated Legendre functions as given in Felderhof's paper (2015).

The deformation ξ may be written analogously as

$$\boldsymbol{\xi} = \sum_{l=1}^{\infty} M_l(t)\mathbf{u}_l(a,\,\theta) + \sum_{l=2}^{\infty} K_l(t)\mathbf{v}_l(a,\,\theta). \tag{23}$$

The deformation has both radial and tangential components and describes an arbitrary axisymmetric deformation of the spherical surface. For periodic deformation with period $T_c = 2\pi/\omega$ we put

$$M_l(t) = a(\mu_{l_s}\cos\omega t - \mu_{l_c}\sin\omega t), \tag{24}$$

$$K_l(t) = a(\kappa_{l_s}\cos\omega t - \kappa_{l_c}\sin\omega t) \tag{25}$$

with dimensionless coefficients μ_{ls}, μ_{lc}, κ_{ls}, κ_{lc}.

The flow velocity has been expanded in powers of the deformation ξ. The first-order velocity $\mathbf{v}^{(1)}(\mathbf{r},\,t)(=\mathrm{u}^{(1)}(\mathbf{r},\,t)+\mathrm{v}^{(1)}(\mathbf{r},\,t))$ is given by

$$\mathbf{v}^{(1)}(\mathbf{r},\,t) = -a\omega\left[\sum_{l=1}^{\infty}\mu_l(t)\mathbf{u}_l(r,\,\theta) + \sum_{l=2}^{\infty}\kappa_l(t)\mathbf{v}_l(r,\,\theta)\right], \tag{26}$$

with the coefficients

$$\mu_l(t) = \mu_{l_c}\cos\omega t + \mu_{l_s}\sin\omega t, \tag{27}$$

$$\kappa_l(t) = \kappa_{l_c}\cos\omega t + \kappa_{l_s}\sin\omega t. \tag{28}$$

For the combined stroke swimmer the values of the coefficients are $\kappa_{2s} = \frac{5}{3}\left(\frac{230}{413}\right)^{1/2}\mu_{1c}$ and $\kappa_{3c} = -\frac{27}{59}\mu_{1c}$. The value of μ_{1c} can freely be chosen; it determines the amplitude of the deformation of the swimmer. The dimensionless amplitude is chosen as $\epsilon = \mu_{1c}$. All other coefficients are 0. According to first-order perturbation calculation there is no net flow velocity of the swimmer. Only in second-order perturbation calculation a net flow velocity occurs (see Felderhof 2015).

The deformation of the combined stroke swimmer (as calculated from equation (23)) as a function of time t/T_c for several time steps is shown in figure 1. More details are given in the introduction.

The first-order flow velocity $u^{(1)}(\mathbf{r},\,t)$ at $t/T_c = 1$ as calculated from Felderhof's (2015) equation (26) is shown in the contour plot of figure 2 as a function of the dimensionless coordinates z/a and r/a . As can be seen this velocity decreases very quickly as a function of the distance from the swimmer. So when making numerical calculations it is important that the number of grid points close to the swimmer is sufficient large.

The combined stroke swimmer as given by Felderhof (2015) deforms in such a way that its volume is not conserved. The deviation in its volume is small (say 2% at $\mu_{1c} = 0.025$). In terms of the perturbation expansion theory the volume is constant to first order in the small deformation parameter ϵ with volume changes occurring only in second order in ϵ. We have corrected this effect. At each time step of the simulation we kept the volume the same.

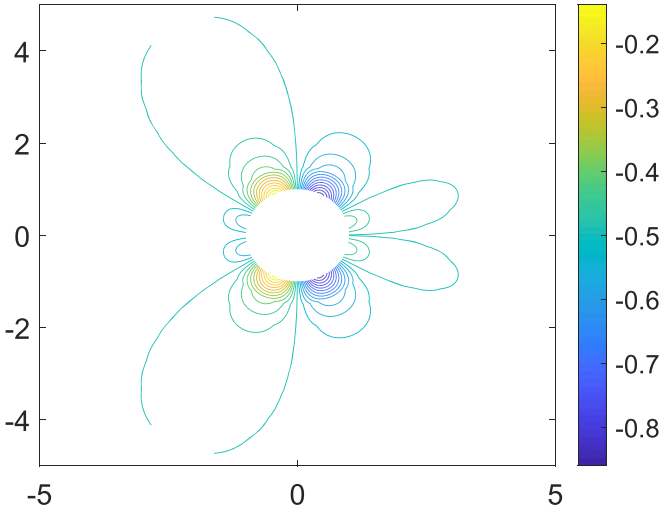

Figure 2. First-order flow velocity $u^{(1)}(\mathbf{r}, t)$ at $t/T_c = 1$.

4. Results

The dimensionless scaling number s of Felderhof and Jones (2017) has been used. s is defined by the radius of the sphere a, the time period of the swimmer T_c and the kinematic viscosity of the fluid ν: $s = a\,(\pi/T_c\nu)^{1/2}$. As mentioned it is similar to the oscillatory Reynolds number $R_\omega = L^2/\nu T$ discussed by Ishimoto (Ishimoto 2013). s can also be defined by the ratio of the radius a of the swimmer and the Stokes length $St_L = (\nu/\omega)^{1/2}$: $s = \frac{1}{\sqrt{2}}\,\frac{a}{St_L}$. So s is a measure of the ratio of swimmer radius and the fluid boundary layer present at the surface of the swimmer. For large values of (say $s = 50$) the boundary layer is thin. In that case the mesh size has to be very small close to the swimmer.

s is a measure of the inertia. Using a different combination of a, T_c and ν with the same value of s gives the same result for the numerical simulation, when also the value of the deformation amplitude ϵ is kept the same. For instance, we used twice the value of T_c and half the value of ν (with the same value of a and ϵ) and found the same velocity distribution and mean velocity for the swimmer.

Transient calculations have been performed. $t = 0$ is the state of rest from which the swimmer starts. Usually four cycles of oscillation are sufficient before time average quantities are calculated to compare with the theoretical averages. However this is not always the case. For instance for $s = 500$ and $\epsilon = 0.050$ the average velocity is still developing. We will discuss the results for the dimensionless mean velocity and the oscillating velocities of the swimmer for two values of the dimensionless deformation amplitude ($\epsilon = 0.025$ and $\epsilon = 0.050$) and three values of s ($s = 0.79$, $s = 50$ and $s = 500$) and compare them with the analytical results of Felderhof and Jones (2017) and Felderhof and Jones (2019). The values of s were chosen in such a way, that for $s = 0.79$ we expected a rather thick boundary layer and for $s = 50$ and $s = 500$ a decreasing boundary layer thickness which for $s = 500$ could become even very thin. For the dimensionless deformation amplitude we first tried a value of $\epsilon = 0.025$ and found it to be in agreement with the analytical results. Thereafter we choose a value $\epsilon = 0.050$ to study possible deviations of the analytical results.

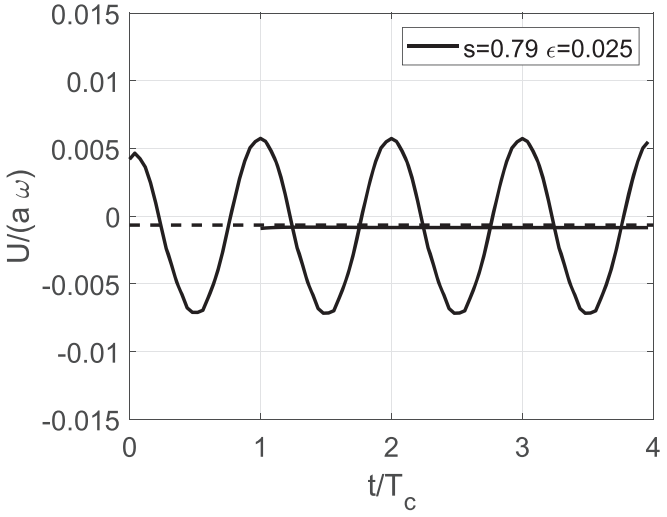

Figure 3. Comparison between numerical and analytical results for the dimensionless mean velocity of the swimmer as function of the dimensionless time for $\epsilon = 0.025$ and $s = 0.79$. Also the numerical result for the dimensionless oscillating velocity of the swimmer as function of the dimensionless time is shown. Full lines: mean velocity and oscillating velocity for numerical calculation. Dotted line: mean velocity for analytical calculation.

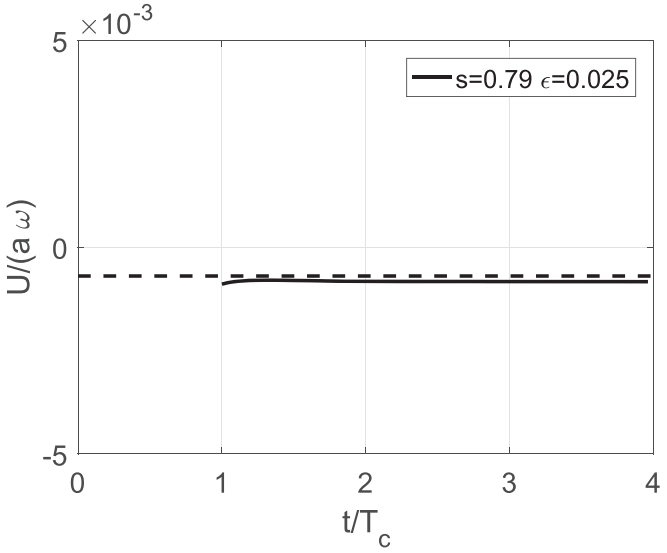

Figure 4. Enlargement of figure 3. Full line: mean velocity for numerical calculation. Dotted line: mean velocity for analytical calculation.

In figures 3–6 a comparison is shown between numerical and analytical results for the dimensionless mean velocity of the swimmer as function of the dimensionless time for $\epsilon = 0.025$ and $\epsilon = 0.050$ at a value of $s = 0.79$. Also the numerical result for the dimensionless oscillating velocity of the swimmer as function of the dimensionless time is shown.

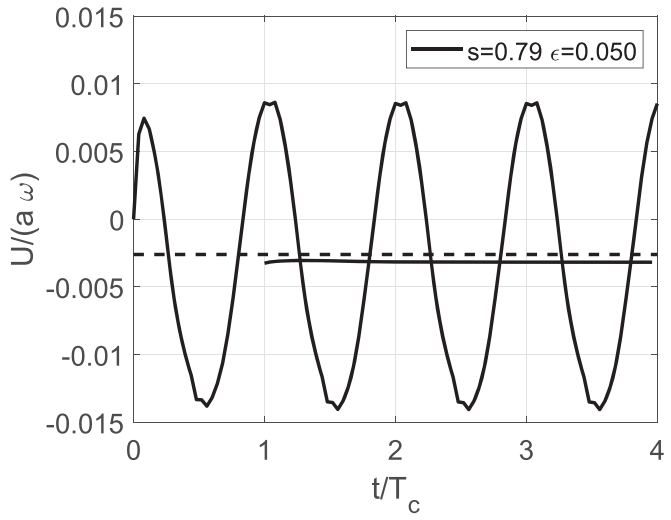

Figure 5. Comparison between numerical and analytical results for the dimensionless mean velocity of the swimmer as function of the dimensionless time for $\epsilon = 0.050$ and $s = 0.79$.

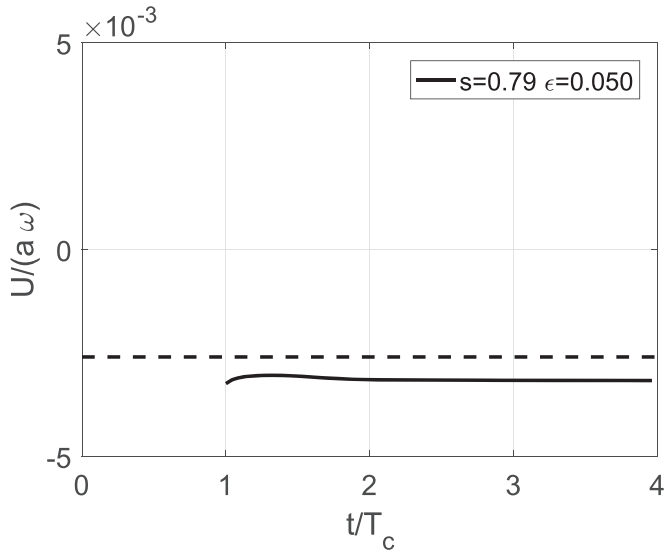

Figure 6. Enlargement of figure 5. Full line: mean velocity for numerical calculation. Dotted line: mean velocity for analytical calculation.

This is also done in figures 7–10 for $\epsilon = 0.025$ and $\epsilon = 0.050$ at a value of $s = 50$; and in figures 11–14 for $\epsilon = 0.025$ and $\epsilon = 0.050$ at a value of $s = 500$. As mentioned the calculations are carried out in the reference system that is at rest with the swimmer. So the velocities have been chosen at a large distance from the swimmer. At this distance the velocities do not change anymore as a function of position.

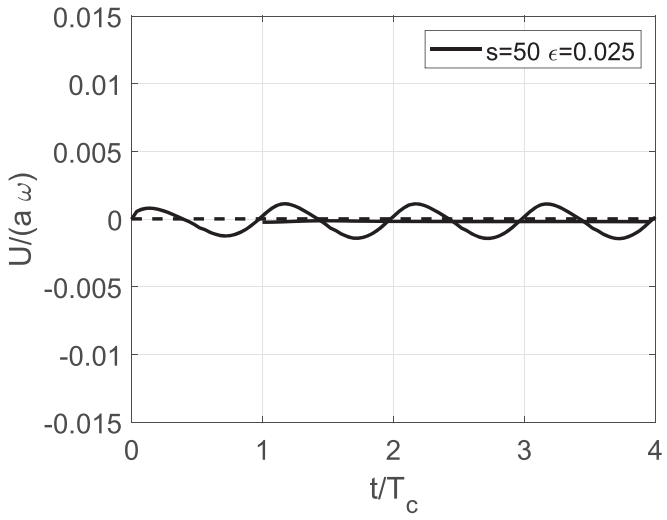

Figure 7. Comparison between numerical and analytical results for the dimensionless mean velocity of the swimmer as function of the dimensionless time for $\epsilon = 0.025$ and $s = 50$.

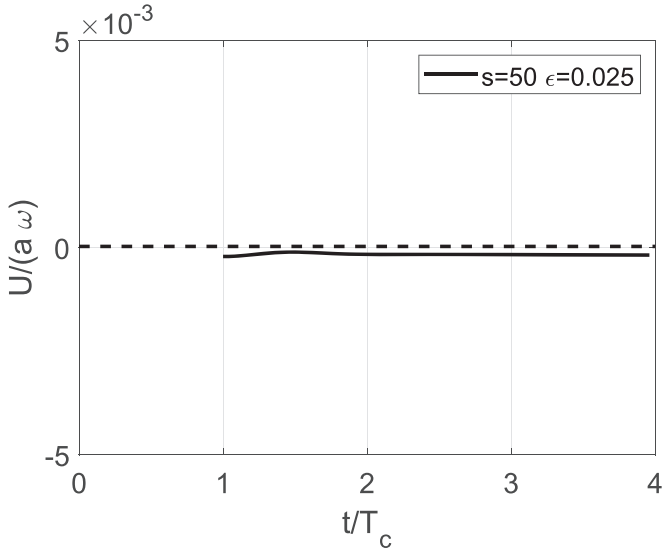

Figure 8. Enlargement of figure 7. Full line: mean velocity for numerical calculation. Dotted line: mean velocity for analytical calculation.

1. For all cases it is found that the oscillating velocity is always much larger than the mean velocity and that for each value of s the oscillating velocity increases with the amplitude of the deformation of the swimmer. That will be discussed in more detail in a later section.

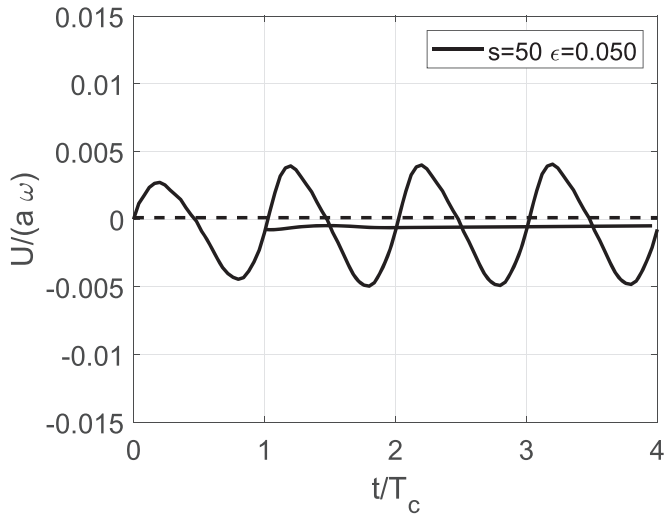

Figure 9. Comparison between numerical and analytical results for the dimensionless mean velocity of the swimmer as function of the dimensionless time for $\epsilon = 0.050$ and $s = 50$.

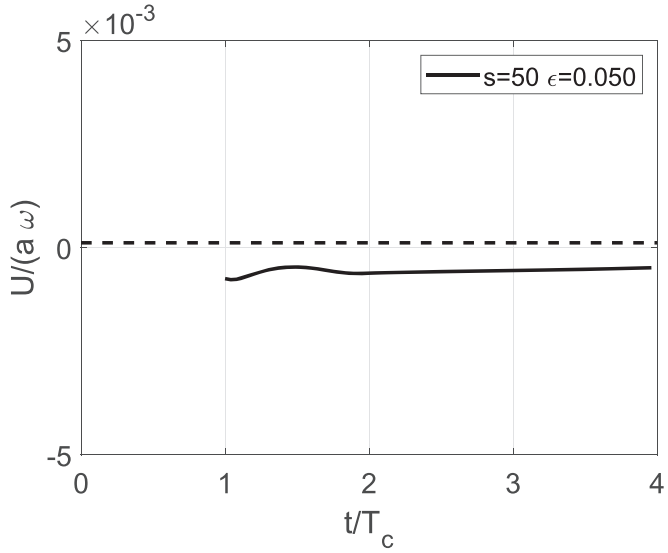

Figure 10. Enlargement of figure 9. Full line: mean velocity for numerical calculation. Dotted line: mean velocity for analytical calculation.

2. The theoretical mean velocity decreases as function of s for both values of the deformation amplitude $\epsilon = 0.025$ and $\epsilon = 0.050$. The numerical mean velocity decreases also as function of s for $\epsilon = 0.025$, but not for $\epsilon = 0.050$.
3. For all three cases of s ($s = 0.79$, $s = 50$, $s = 500$) we found for the lowest value of the deformation amplitude $\epsilon = 0.025$ a very good agreement for the mean velocity between the numerical and theoretical results. However, for all three cases of s at the largest value

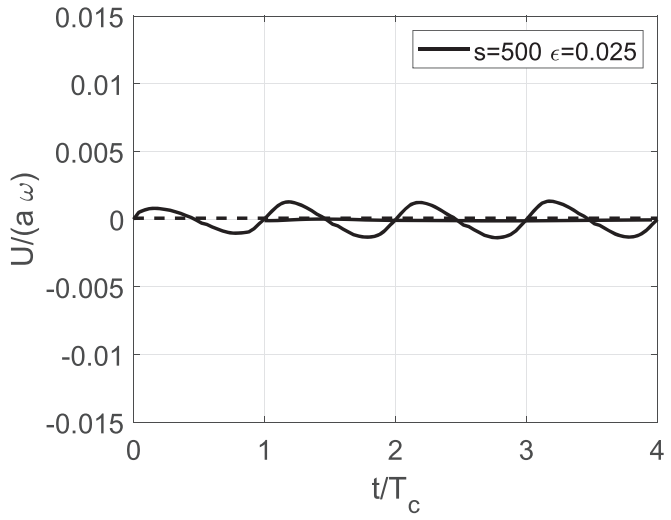

Figure 11. Comparison between numerical and analytical results for the dimensionless mean velocity of the swimmer as function of the dimensionless time for $\epsilon = 0.025$ and $s = 500$.

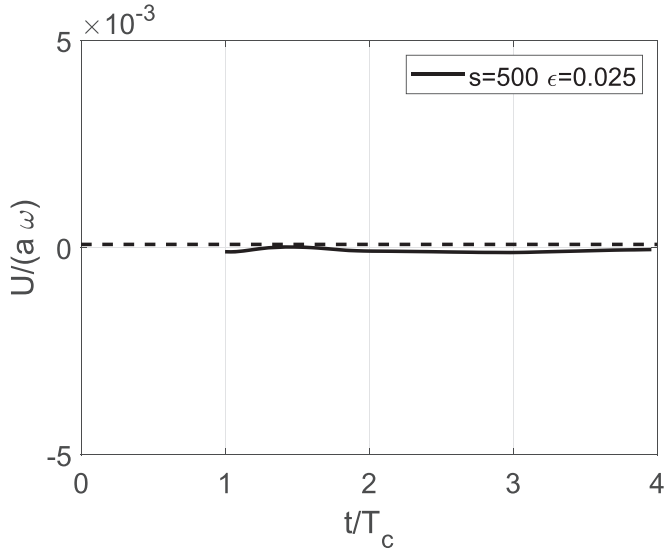

Figure 12. Enlargement of figure 11. Full line: mean velocity for numerical calculation. Dotted line: mean velocity for analytical calculation.

of the deformation amplitude $\epsilon = 0.050$ there is a deviation between the mean velocity of the numerical and theoretical results. The increase of a factor of two in the deformation amplitude ϵ has a marked influence on the results, in particular for the case that $s = 500$ (which is still developing as a function of time). This is due to the influence of inertia. We checked this by repeating the numerical calculation for the case ($\epsilon = 0.050$, $s = 500$) but

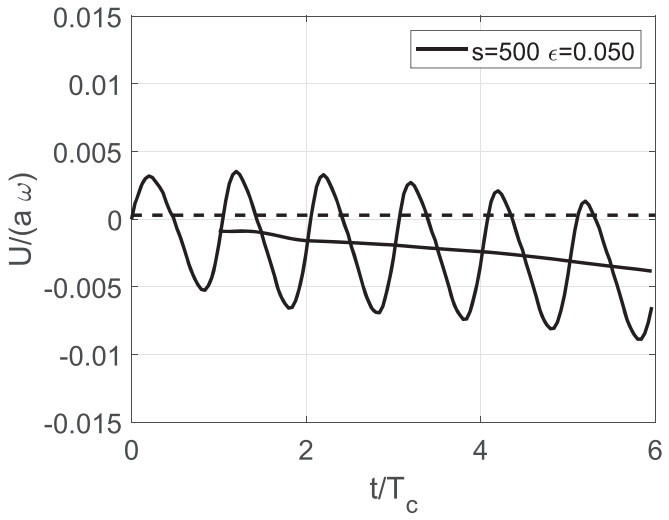

Figure 13. Comparison between numerical and analytical results for the dimensionless mean velocity of the swimmer as function of the dimensionless time for $\epsilon = 0.050$ and $s = 500$.

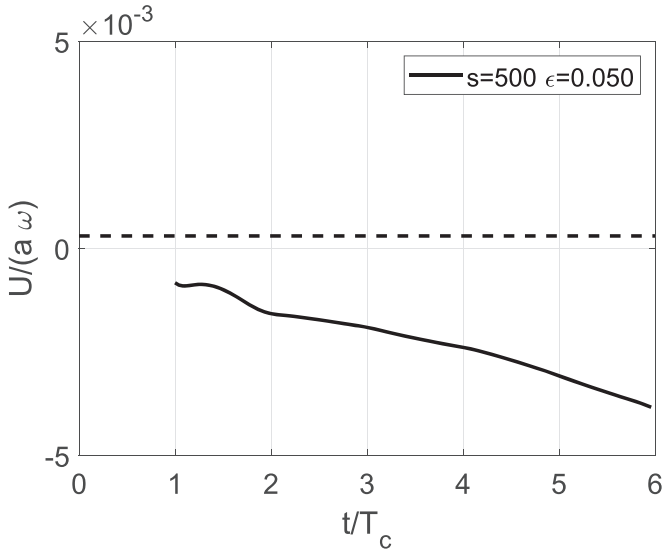

Figure 14. Enlargement of figure 13. Full line: mean velocity for numerical calculation. Dotted line: mean velocity for analytical calculation.

now without inertial advective term in the Navier–Stokes equation. Indeed we confirmed that then the mean velocity is much smaller (0.000 32).

In figures 15 and 16 we compare the oscillating velocities of the swimmer at small ($\epsilon = 0.025$) and large ($\epsilon = 0.050$) values of the deformation amplitude and three value of scale number ($s = 0.79$, $s = 50$ and $s = 500$) with the prediction made by Felderhof and Jones (2018). As can be seen the theoretical and numerical results agree well for ($s = 50$ and

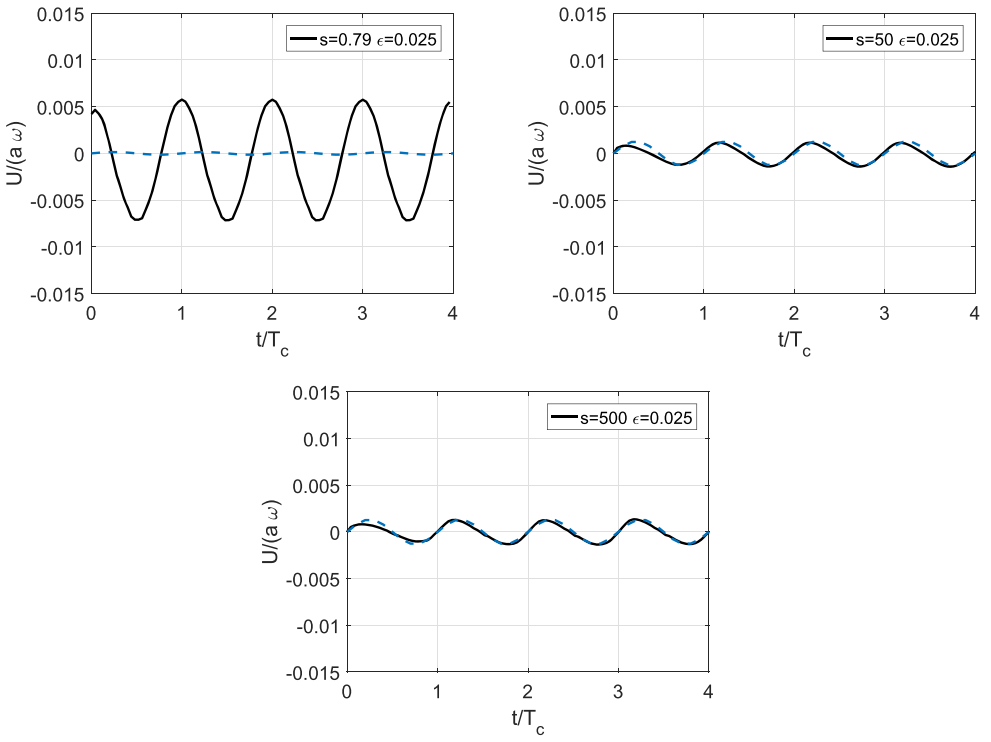

Figure 15. Full line: numerical value of the dimensionless oscillating velocity for $s = 0.79$, $s = 50$ and $s = 500$ and for $\epsilon = 0.025$. The dashed lines are the values according to the theoretical predictions of Felderhof and Jones (2018).

$s = 500$) at a small amplitude ($\epsilon = 0.025$). At a large value of the deformation amplitude ($\epsilon = 0.050$) the results at $s = 50$ and $s = 500$ differ significantly between numerical simulation and theoretical prediction, in agreement with the results for the mean velocity. For $s = 0.79$ the results for the numerical simulation and the theoretical caculation differ very much. The numerical values for the oscillating velocity are then much larger than the theoretical ones at both small ($\epsilon = 0.025$) and large ($\epsilon = 0.050$) values of the deformation amplitude. We checked our calculation carefully, but have no explanation.

A stream traces filter has been used to generate streamlines in a vector flow field from a number of arbitrarily chosen seed points. In figure 17 we show the streamlines in the reference frame of the swimmer for $\epsilon = 0.050$ and $s = 0.79$ at $t/T_c = 3$ and $t/T_c = 11/3$ and for $\epsilon = 0.050$ and $s = 50$ also at $t/T_c = 3$ and $t/T_c = 11/3$. If a Reynolds number is defined based on the mean swimming velocity, we find for ($\epsilon = 0.050$ and $s = 0.79$) $Re_m = 0.0035$ and for ($\epsilon = 0.050$ and $s = 50$) $Re_m = 1.05$. So for ($\epsilon = 0.050$ and $s = 0.79$) the flow is in Stokes regime with negligible effect of inertia, whereas for ($\epsilon = 0.050$ and $s = 50$) the inertia has an influence. So it is interesting to compare the results. As can be seen at $Re_m = 0.0035$ the streamlines run smoothly around the swimmer (there is only a small recirculating region), whereas at $Re_m = 1.05$ the streamlines show large recirculating regions. It has to be understood that the definition of Re_m is rather arbitrary considering the large oscillating velocities.

The recirculating regions are reminiscent of figure 4 of Chisholm *et al* (2016). However there is a difference: the streamlines in Chisholm *et al* (2016) are constant in time and position

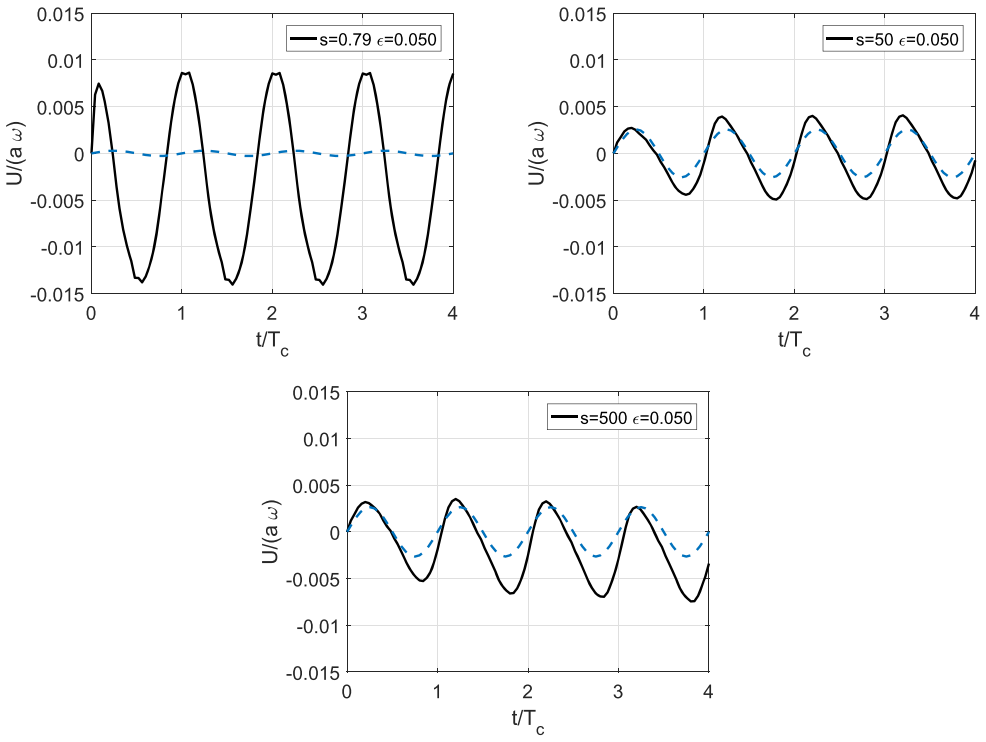

Figure 16. Full line: numerical value of the dimensionless oscillating velocity for $s = 0.79$, $s = 50$ and $s = 500$ and for $\epsilon = 0.050$. The dashed lines are the values according to the theoretical predictions of Felderhof and Jones (2018).

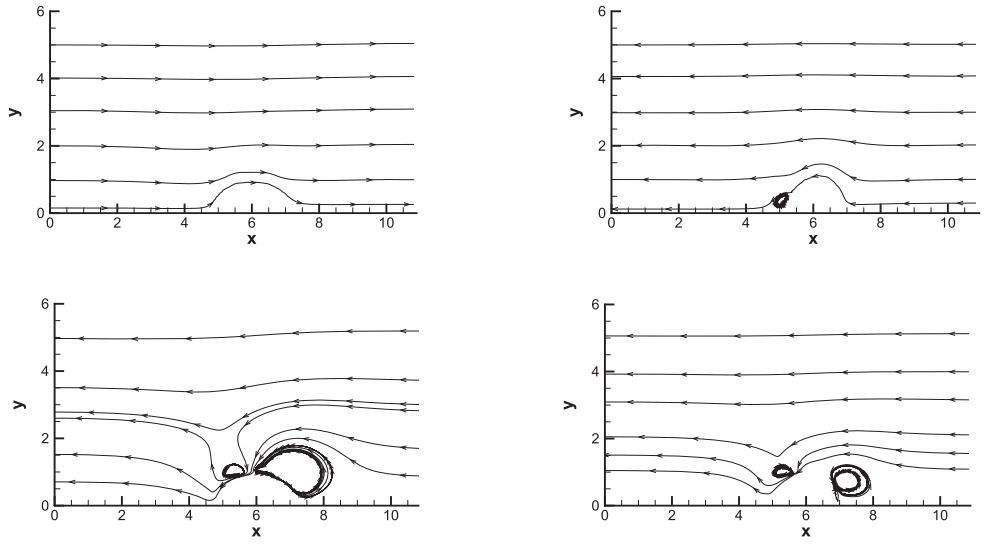

Figure 17. Streamlines. top: for $s = 0.79$ and $\epsilon = 0.050$ at $t/T_c = 3$ and $t/T_c = 11/3$; bottom: for $s = 50$ and $\epsilon = 0.050$ at $t/T_c = 3$ and $t/T_c = 11/3$. $x = z/a$ and $y = r/a$.

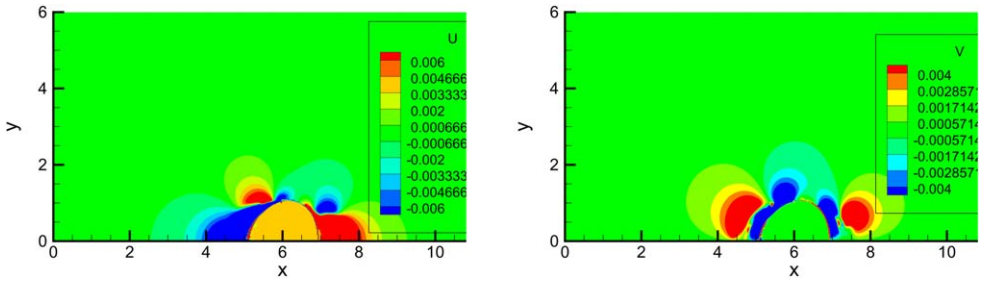

Figure 18. Contour plots for the dimensionless U- and V-velocity for the case $\epsilon = 0.050$ at $t/T_c = 11/3$ (see figure 17).

whereas the streamlines in figure 17 are changing in time and position due to the oscillating velocity.

In figure 18 we show the dimensionless U-contour in x-direction and the V-contour in y-direction for the case $\epsilon = 0.050$ at $t/T_c = 11/3$ (see figure 17) for the reference system with the fluid at rest at large distance from the swimmer. The nine digits of numerical precision included in the legend have been chosen so that the velocity of the swimmer can be observed. The U-velocity shows that the dimensionless swimmer velocity is about 0.005. The fluid velocity decreases with increasing distance from the swimmer and becomes equal to zero everywhere else. The V-velocity shows positive and negative parts close to the swimmer and zero at larger distances from the swimmer.These results are due to the strong recirculating flow close to the swimmer.

5. Conclusion

An important conclusion is that the numerical value of the mean velocity of the swimmer agrees well with the theoretical value when the amplitude of the deformation of the swimmer is small. At larger values of the amplitude of the swimmer the results for the theory and numerical calculation deviate. This is to be expected, as the theory is based on a perturbation calculation. This holds also for the oscillating velocity at $s = 50$ and $s = 500$. Based on these findings our conclusion is, that in future calculations our code can be used with trust also for larger deformation amplitudes.

As discussed, for $s = 0.79$ the results for the numerical oscillating velocity are much larger than the theoretical ones at both small ($\epsilon = 0.025$) and large ($\epsilon = 0.050$) values of the deformation amplitude. We also compared our numerical simulation with two different codes: our own Fortran code (using IBM) and the commercial Fluent code (using the dynamic mesh method). For both cases we found that for $s = 0.79$ the results for the numerical oscillating velocity are much larger than the theoretical ones.

In the future our intention is to study in even more detail the dependency of the swimmer velocity on the amplitude of the deformation of the swimmer. Will there be a limit in the swimmer velocity? A first calculation has been made for the case $\epsilon = 0.075$; $s = 500$ (figure 19). As can be seen from the comparison between (figure 11), (figure 13) and (figure 19) the mean velocity is still increasing strongly with the amplitude of the deformation.

The axisymmetric code can rather easily be extended into a three-dimensional one. Several interesting phenomena can then be studied, for instance the movement of the

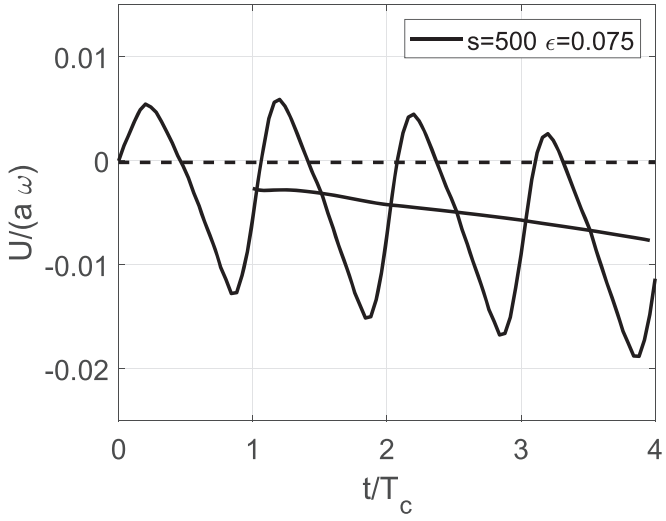

Figure 19. Comparison between numerical and analytical results for the dimensionless mean velocity of the swimmer as function of the dimensionless time for $\epsilon = 0.075$ and $s = 500$.

swimmer close to a solid boundary or the interaction between swimmers. We will then also study the range of validity of the assumption of axisymmetric flow for the case where inertia is important.

The velocity of the swimmer shows large oscillations. These oscillations are considerably larger than the mean swimming velocity.

At a small value of inertia the streamlines show a smooth and gradual behaviour as a function of time and distance from the swimmer. At a significant larger value of inertia the streamlines show recirculating regions.

The model of Felderhof (2015) can be used to analyze the swimming of a spherical micro-organism. In the model the deformation of a sphere is described analytically as a function of time using perturbation theory. Different types of swimmers can be obtained by using different combinations for the coefficients describing the deformation. The combined stroke swimmer used here is an example of this.

References

Chisholm N G, Legendre D, Lauga E and Khair A S 2016 A squirmer across Reynolds numbers *J. Fluid Mech.* **796** 233–56

Dombrowski T, Jones S K, Katsikis G, Bhalla A P S, Griffith B E and Klotsa D 2019 Transition in swimming direction in a model self-propelled inertia swimmer *Phys. Rev. Fluids* **4** 021101(R)

Felderhof B U 2015 Stokesian spherical swimmer and active particle *Phys. Rev.* E **91** 043018

Felderhof B U and Jones R B 2017 Swimming of a sphere in a viscous incompressible fluid with inertia *Fluid Dyn. Res.* **49** 045510

Felderhof B U and Jones R B 2018 Swimming of a uniform deformable sphere in a viscous incompressible fluid with inertia arXiv:1811.07116v1 [physics.flu -dyn]

Felderhof B U and Jones R B 2019 Effect of fluid inertia on swimming of a sphere in a viscous incompressible fluid *Eur. J. Mech.* B **75** 312–26

Ishimoto K 2013 A spherical squirming swimmer in unsteady Stokes flow *J. Fluid Mech.* **723** 163–89

Kajishima T, Takiguchi S, Hamasaki H and Miyake Y 2001 Turbulence structure of particle-laden flow in a vertical plane channel due to vortex shedding *JMSE Int. J.* B **44** 526–35

Khair A S and Chisholm N G 2014 Expansions at small Reynolds numbers for the locomotion of a spherical squirmer *Phys. Fluids* **26** 01190

Li G-J and Ardekani M 2014 Hydrodynamic interaction of micro-swimmers near a wall *Phys. Rev.* E **90** 013010

Wang S and Ardekani A 2012 Inertial squirmer *Phys. Fluids* **24** 101902